Supplement of Atmos. Chem. Phys., 25, 12037–12049, 2025
https://doi.org/10.5194/acp-25-12037-2025-supplement

Atmospheric Chemistry and Physics
Open Access
EGU

Supplement of

Measurement report: simultaneous measurement on gas- and particle-phase water-soluble organics in Shanghai: enhanced light absorption of transported Asian dust

Zheng Li et al.

Correspondence to: Gehui Wang (ghwang@geo.ecnu.edu.cn) and Can Wu (cwu@geo.ecnu.edu.cn)

Text S1 Detailed description of the instruments

The ambient air was sampled and separated by a $PM_{2.5}$ sharp cut cyclone with a flow rate of 16.7 L/min. Then, the air was drawn through the passageway between the inner and outer Pyrex glass tubes in wet annular denuder (WAD) system. In WAD system, gaseous samples were wetted with pure water and collected. Scrub and Impact Aerosol Collector (SIC) was placed downstream of the WAD for collecting aerosol phase samples. The gas and aerosol samples were subsequently injected into the ion chromatography (ICS-5000+, Themo Scientific) for analysis of water-soluble inorganic ions and small molecular organic acids after removing the insoluble species and bubbles.

The gas and particle-phase water-soluble organic carbon and water-soluble organic nitrogen (WSOC/WSON) were simultaneous determined by using a TOC/TN analyzer (TOC-L CPH, Shimadzu, Japan). The concentrations of WSOC were calculated as the difference between water-soluble total carbon (WSTC) and water-soluble inorganic carbon (WSIC). Similar, the concentrations of WSON were calculated as the difference between water-soluble total nitrogen (WSTN) and water-soluble inorganic nitrogen (WSIN).

Organic carbon (OC) and elemental carbon (EC) were determined by DRI Model 2015 Carbon Analyzer (Atmoslytic, Inc., Calabasas, USA) with IMPROVE_A protocol (Chow et al., 2007).

Text S2 Absorption spectra of water-soluble BrC analysis

The light absorption spectra of the water-soluble BrC was measured by a UV-vis spectrometer (T6 New Century, Persee) over a wavelength range of 200 − 900 nm (Wu et al., 2024). The light absorption coefficients (Abs_{λ}, M m^{-1}) of the water extracts was calculated by eq (1).

$$\mathrm{Abs}_\lambda = (A_\lambda - A_{700})\ \frac{V_l}{V_a \times l} \times \ln(10) \quad (1)$$

where A_λ and A_{700} represent the light absorption at the wavelengths of λ and 700 nm measured by the UV-vis spectrometer. V_l refers to the volume of solvent extract. V_a refers to the sampling volume and l corresponds to the path length of the cell (1 cm).

The mass absorption coefficient (MAC_λ, $m^2\ g^{-1}$) of the extracts at the wavelength of λ can be quantified as eq (2)

$$\mathrm{MAC}_\lambda = \frac{\mathrm{Abs}_\lambda}{M} \quad (2)$$

where M represent the concentration of WSOC.

The MAC of IMs standards in the water solvent at a wavelength of λ can be calculated as in Laskin et al (2015):

$$\mathrm{MAC}_{i,\lambda} = \frac{A_\lambda - A_{700}}{l \times C_i}\ln(10) \quad (3)$$

where C_i (mg L^{-1}) is the concentration of the i compound standards in the water solvent.

The light absorption contribution of IMs to BrC at a wavelength of λ can be obtained using eq (4):

$$\mathrm{Cont}_{i/\mathrm{BrC},\lambda} = \frac{MAE_{i,\lambda} \times C_i}{Abs_{BrC,\lambda}} \quad (4)$$

where the C_i (μg m^{-3}) is the atmospheric concentration of i compound, and the $Abs_{BrC,\lambda}$ is the absorption coefficient of water-soluble BrC at a wavelength of λ.

Text S3 Contribution of organic matter to aerosol liquid water content (ALWC)

Here we used the ALWC calculation method reported by Lv et al (2022b; 2022a). The contribution of organic matter (OM) to ALWC ($ALWC_{org}$) were defined as the following eq (3)

$$\mathrm{ALWC}_{org} = \frac{[OM]\rho_W}{\rho_{org}}\ \frac{\kappa_{org}}{\frac{1}{RH} - 1} \quad (5)$$

where OM is the mass concentration of organics, ρ_w is the density of water, ρ_{org} is the

density of OM (1.4 g cm^{-3}). κ_{org} is the hygroscopicity parameter of OM (0.06).

Table S1. Relative abundances (%) of ammonium, nitrate, and sulfate in $PM_{2.5}$ or PM_{10} during dust storm periods in different regions of China.

Sampling site		Sampling time	NH_4^+	NO_3^-	SO_4^{2-}	Type	Reference
Desert region	Tengger	03, 2023	0.03	0.5	4.1	PM_{10}	This study
	Taklimakan	04, 2008	-	0.3	4.2	$PM_{2.5}$	(Wu et al., 2012)
Upwind region	Xi'an	2017	0.3	0.9	1.8	TSP	(Wu et al., 2019)
	Wuhai	03, 2021	0.4	0.7	1.1	$PM_{2.5}$	(Li et al., 2023)
Downwind region	Shanghai	10, 2019	3.8	10.1	6.4	$PM_{2.5}$	(Wu et al., 2020)
	Shanghai	03-04, 2023	3.3	8.1	5.3	$PM_{2.5}$	This study

Table S2. Concentrations of water-soluble inorganic ions and organic acids in Shanghai during spring of 2023.

	Whole campaign	Dust storm	Haze event	Clean period
I Gaseous pollutants				
Formic $acid_g$[a] (μg m^{-3})	3.2 ± 4.4	1.5 ± 2.6	1.3 ± 1.0	3.4 ± 6.7
Acetic $acid_g$[a] (μg m^{-3})	1.2 ± 2.3	0.9 ± 2.0	0.5 ± 0.4	1.3 ± 2.8
NH_3 (μg m^{-3})	4.9 ± 1.6	5.1 ± 1.6	4.0 ± 0.8	5.3 ± 1.8
II Major components of $PM_{2.5}$				
OC (μgC m^{-3})	5.0 ± 2.7	6.0 ± 5.0	5.7 ± 1.9	3.8 ± 3.2
$WSOC_p$/OC	0.6 ± 0.2	0.5 ± 0.2	0.7 ± 0.1	0.7 ± 0.1
EC (μgC m^{-3})	1.1 ± 0.6	0.7 ± 0.4	1.1 ± 0.5	0.7 ± 0.5
Formic $acid_p$[a] (μg m^{-3})	0.2 ± 0.1	0.1 ± 0.1	0.3 ± 0.1	0.2 ± 0.1
Acetic $acid_p$[a] (μg m^{-3})	0.06 ± 0.04	0.04 ± 0.04	0.1 ± 0.04	0.06 ± 0.04
Oxalic $acid_p$[a] (μg m^{-3})	0.3 ± 0.3	0.2 ± 0.3	0.5 ± 0.4	0.3 ± 0.2
Na^+ (μg m^{-3})	0.2 ± 0.3	0.4 ± 0.1	0.1 ± 0.05	0.2 ± 0.2
Mg^{2+} (μg m^{-3})	0.08 ± 0.06	0.2 ± 0.05	0.04 ± 0.01	0.1 ± 0.02

[a]Formic $acid_g$ and acetic $acid_g$ are the gas-phase organics while formic $acid_p$, acetic $acid_p$ and oxalic $acid_p$ are the organics in $PM_{2.5}$.

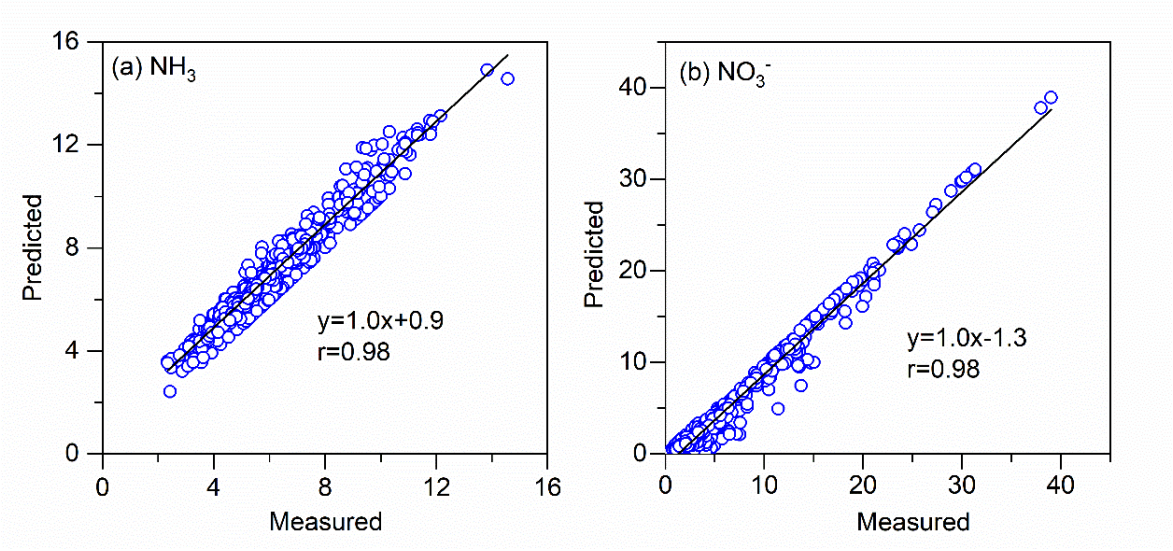

Figure S1. Comparison of measured ammonia and nitrate and predicted by ISORROPIA-II model.

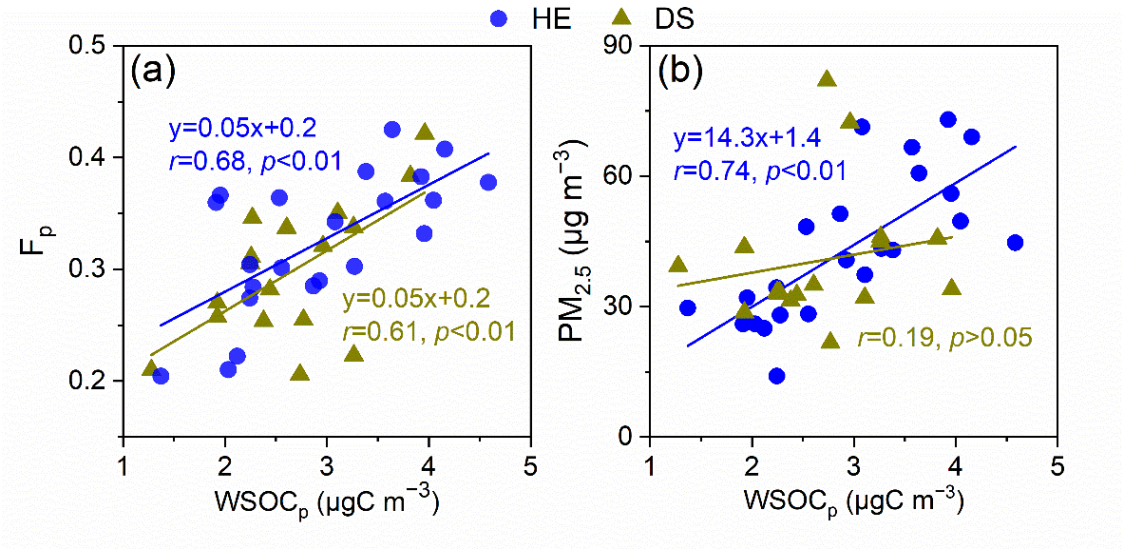

Figure S2. Linear regression analysis for $WSOC_p$ with (a) partitioning coefficient of WSOCs (F_p) and (b) $PM_{2.5}$ during the haze event (HE) and dust storm (DS) event, respectively

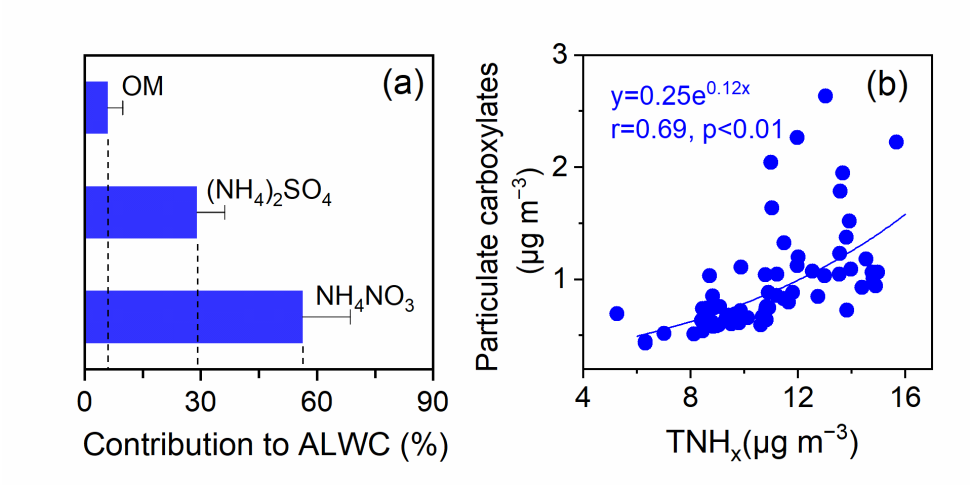

75

76 **Figure S3**. (a) Contributions of NH_4NO_3, $(NH_4)_2SO_4$ and OM to ALWC in the haze
77 event (HE); (b) Particulate carboxylates as a function of TNH_x in the haze event (HE).

78

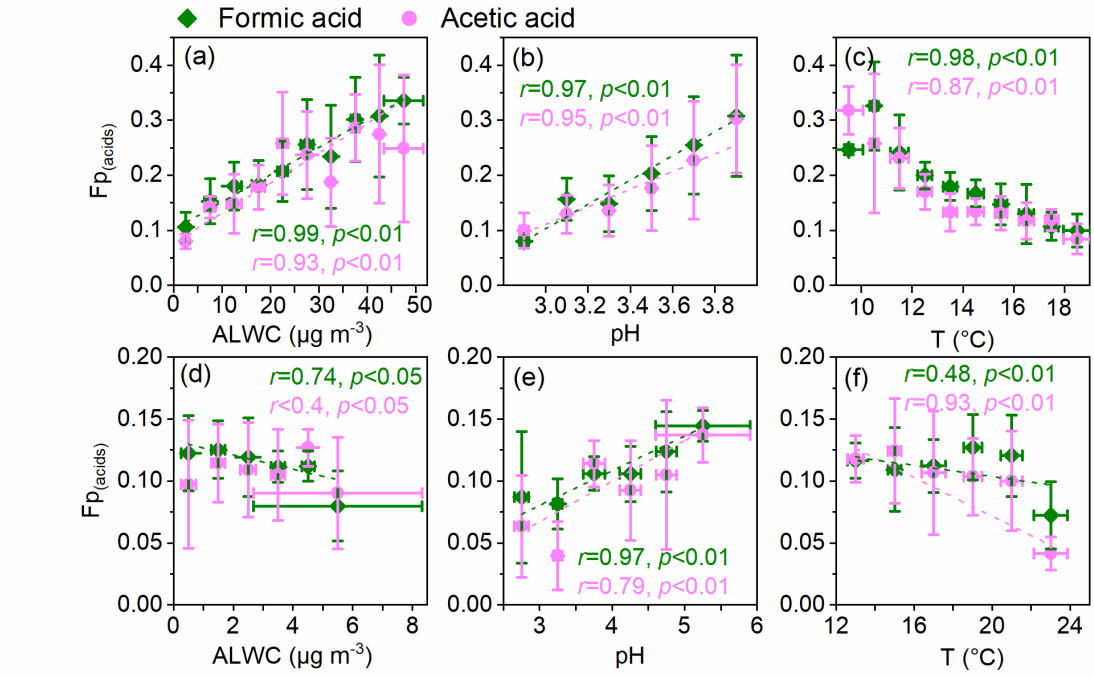

79

80 **Figure S4.** Factors affecting the gas-to-particle partitioning coefficients of formic and
81 acetic acids in (a-c) HE and (d-f) DS periods in spring 2023 in Shanghai.

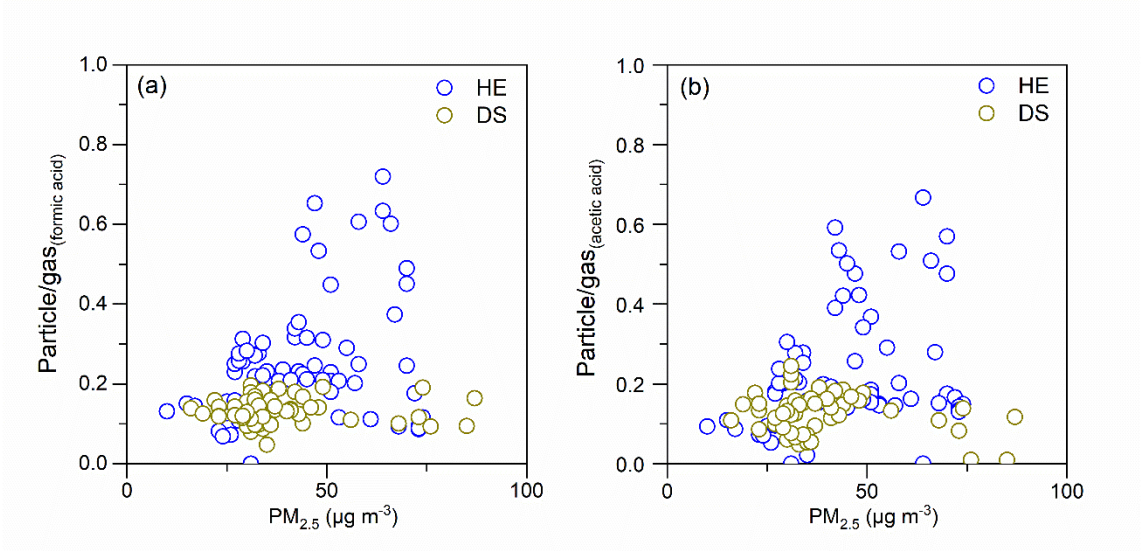

Figure S5. Partitioning coefficients of low molecular organic acids (formic and acetic acids) versus $PM_{2.5}$ during HE and DS periods.

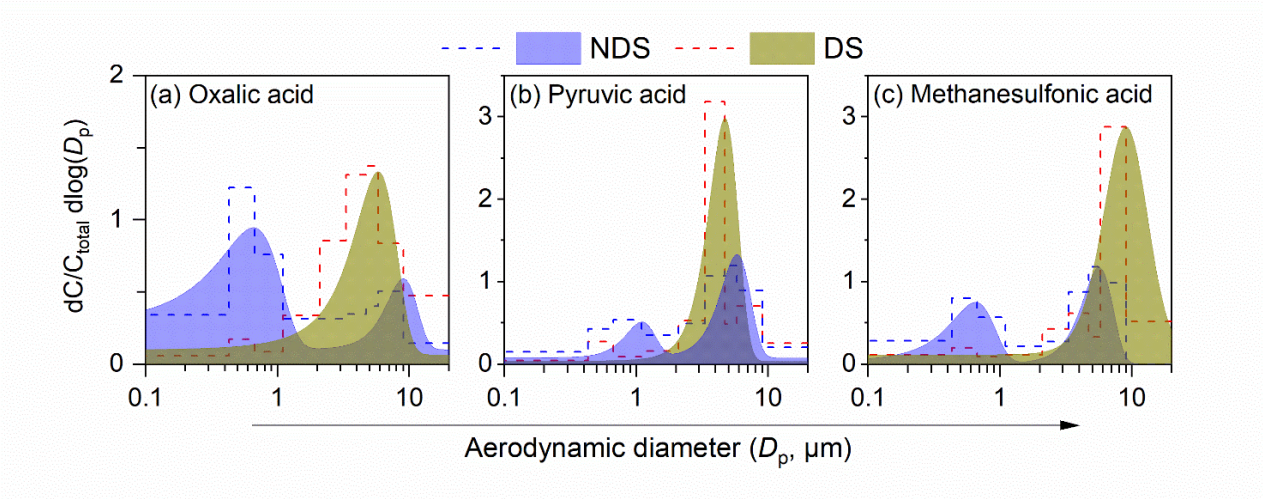

Figure S6. Size distribution of (a) oxalic acid, (b) pyruvic acid and (c) methanesulfonic acid during the non-dust storm (NDS) and dust storm (DS) events in Shanghai. The dashed lines and filled areas are the measured size distribution and fitting results, respectively. C_{total} is the sum of concentration on all the 9-stages.

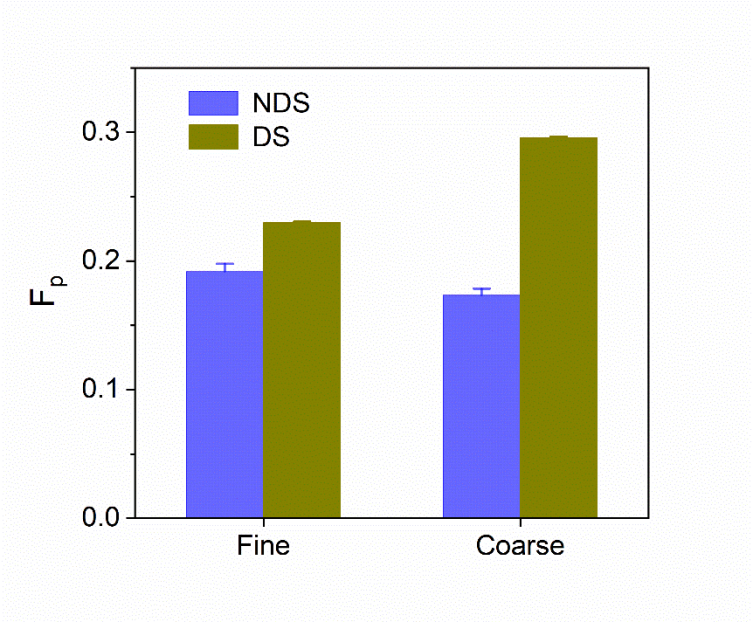

Figure S7. The partitioning coefficients (F_p) of WSOCs in the fine (<2.1μm) and coarse (>2.1μm) in the non-dust storm (NDS) and dust storm (DS) periods in Shanghai during spring of 2023.

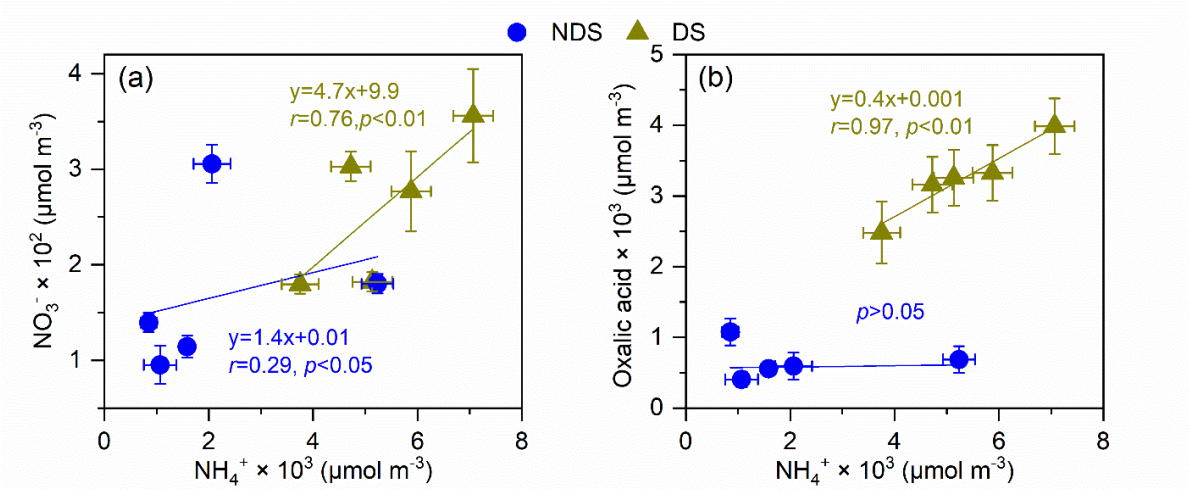

Figure S8. Liner fit regression for the NH_4^+ with (a) NO_3^- and (b) oxalic acid in coarse mode (>2.1 μm) of particles in the non-dust storm (NDS) and dust storm (DS) periods in Shanghai during spring of 2023.

References

Chow, J. C., Watson, J. G., Chen, L. W. A., Chang, M. C. O., Robinson, N. F., Trimble, D., and Kohl, S.: The IMPROVE_A Temperature Protocol for Thermal/Optical Carbon Analysis: Maintaining Consistency with a Long-Term Database, J Air Waste Manage, 57, 1014-1023, https://doi.org/10.3155/1047-3289.57.9.1014, 2007.

Laskin, A., Laskin, J., and Nizkorodov, S. A.: Chemistry of Atmospheric Brown Carbon, Chem. Rev., 115, 4335-4382, https://doi.org/10.1021/cr5006167, 2015.

Li, R., Zhang, M., Du, Y., Wang, G., Shang, C., Liu, Y., Zhang, M., Meng, Q., Cui, M., and Yan, C.: Impacts of dust events on chemical characterization and associated source contributions of atmospheric particulate matter in northern China, Environmental Pollution, 316, 120597, https://doi.org/10.1016/j.envpol.2022.120597, 2023.

Lv, S. J., Wu, C., Wang, F. L., Liu, X. D., Zhang, S., Chen, Y. B., Zhang, F., Yang, Y., Wang, H. L., Huang, C., Fu, Q. Y., Duan, Y. S., and Wang, G. H.: Nitrate-Enhanced Gas-to-Particle-Phase Partitioning of Water- Soluble Organic Compounds in Chinese Urban Atmosphere: Implications for Secondary Organic Aerosol Formation, Environ. Sci. Tech. Let., 10, 14-20, https://doi.org/10.1021/acs.estlett.2c00894, 2022a.

Lv, S. J., Wang, F. L., Wu, C., Chen, Y. B., Liu, S. J., Zhang, S., Li, D. P., Du, W., Zhang, F., Wang, H. L., Huang, C., Fu, Q. Y., Duan, Y. S., and Wang, G. H.: Gas-to-Aerosol Phase Partitioning of Atmospheric Water-Soluble Organic Compounds at a Rural Site in China: An Enhancing Effect of NH3 on SOA Formation, Environ. Sci. Technol., 56, 3915-3924, https://doi.org/10.1021/acs.est.1c06855, 2022b.

Wu, C., Liu, X., Zhang, K., Zhang, S., Cao, C., Li, J., Li, R., Zhang, F., and Wang, G.: Measurement report: Formation of tropospheric brown carbon in a lifting air mass, Atmos. Chem. Phys., 24, 9263-9275, http://doi.org/10.5194/acp-24-9263-2024, 2024.

Wu, C., Wang, G., Cao, C., Li, J., Li, J., Wu, F., Huang, R., Cao, J., Han, Y., Ge, S., Xie, Y., Xue, G., and Wang, X.: Chemical characteristics of airborne particles in Xi'an, inland China during dust storm episodes: Implications for heterogeneous formation of ammonium nitrate and enhancement of N-deposition, Environmental Pollution, 244, 877-884, https://doi.org/10.1016/j.envpol.2018.10.019, 2019.

Wu, C., Zhang, S., Wang, G. H., Lv, S. J., Li, D. P., Liu, L., Li, J. J., Liu, S. J., Du, W., Meng, J. J., Qiao, L. P., Zhou, M., Huang, C., and Wang, H. L.: Efficient Heterogeneous Formation of Ammonium Nitrate on the Saline Mineral Particle Surface in the Atmosphere of East Asia during Dust Storm Periods, Environ. Sci. Technol., 54, 15622-15630, https://doi.org/10.1021/acs.est.0c04544, 2020.

Wu, F., Zhang, D., Cao, J., Xu, H., and An, Z.: Soil-derived sulfate in atmospheric dust particles at Taklimakan desert, Geophys. Res. Lett., 39, https://doi.org/10.1029/2012GL054406, 2012.